Materials & Design 212 (2021) 110228

Contents lists available at ScienceDirect

Materials & Design

journal homepage: www.elsevier.com/locate/matdes

Three-dimensional bioprinting of bioactive scaffolds with thermally embedded abalone shell particles for bone tissue engineering

Dahong Kim [a,b,1], Jihye Lee [a,1], Ji Min Seok [a,b], Joo-Yun Jung [a], Jun Hee Lee [a], Jun Sik Lee [c], Kangwon Lee [b,2,*], Su A Park [a,2,*]

[a] Nano Convergence & Manufacturing Systems, Korea Institute of Machinery and Materials (KIMM), Daejeon 34103, Republic of Korea
[b] Department of Applied Bioengineering, Graduate School of Convergence Science and Technology, Seoul National University, Seoul 08826, Republic of Korea
[c] Department of Life Science, Immunology Research Lab, College of Natural Sciences, Chosun University, Gwangju 61452, Republic of Korea

HIGHLIGHTS

- The bioactive scaffolds were fabricated by a 3D bio-printing method to construct microstructures of abalone shell particles (ASP) containing bioactive factors.
- ASP is thermally embedded on the printed scaffold, and can load heat resistant particles onto the surface and simple control the roughness of the surface.
- The ASP scaffold showed increased viability, proliferation, and differentiation of osteoblast like cells.
- This study shows the possibility of applying bioactive scaffolds to the natural organisms for bon tissue engineering.

GRAPHICAL ABSTRACT

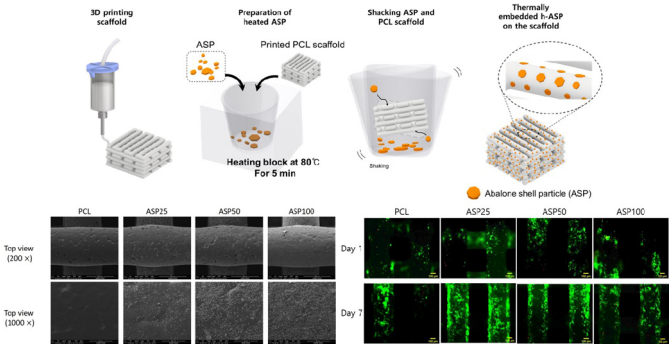

ARTICLE INFO

Article history:
Received 25 April 2021
Revised 19 October 2021
Accepted 7 November 2021
Available online 8 November 2021

Keywords:
Three-dimensional printing
Abalone shell
Bone tissue engineering
Bone scaffold
Bioactive scaffold
Marine organism

ABSTRACT

Abalone shells, which contain both organic and inorganic matter, can facilitate bone remodeling and have been used to fabricate three-dimensional (3D)-printed scaffolds for bone regeneration. Herein, polycaprolactone (PCL) scaffolds were fabricated using 3D printing with abalone shell particles (ASPs) used in high-temperature processing. ASPs were heated to approximately the melting point of PCL and thermally embedded in 3D-printed PCL using a relatively simple process. The morphology and roughness of the composite scaffold changed according to the weight of ASPs used. The scaffolds were grouped as follows: ASP25 (25 mg), ASP50 (50 mg), and ASP100 (100 mg). The ASP25 group exhibited optimum cell viability and proliferation because of the direct influence of roughness and rapid pH changes. The ASP25 and ASP100 groups showed the highest alkaline phosphatase activity. This could be attributed to the effect of the alkaline environment, dissolution of calcium ions, and presence of bioactive molecules in the ASPs that could support bone regeneration. Therefore, the ASP25 group was the most suitable for fabricating bone scaffolds. This study revealed the potential applicability of ASP-embedded scaffolds in bone

* Corresponding authors at: Department of Applied Bioengineering, Graduate School of Convergence Science and Technology, Seoul National University, Seoul 08826, Republic of Korea (Kangwon Lee) and Department of Nature-Inspired Nano Convergence Systems, Nano Convergence & Manufacturing Systems Korea Institute of Machinery and Materials (KIMM), Daejeon 34103, Republic of Korea (Su A Park).
E-mail addresses: kangwonlee@snu.ac.kr (K. Lee), psa@kimm.re.kr (S.A Park).
[1] These co-authors contributed equally to this work.
[2] These corresponding authors contributed equally to this work.

https://doi.org/10.1016/j.matdes.2021.110228

tissue engineering involving natural bio-organisms that self-mineralize in a process similar to human bone formation.

1. Introduction

Many methods have been used to treat large bone defects, including autografts and allografts. However, these methods are disadvantageous because donors are scarce, and immunogenic rejection and disease-related complications are prone to occur [1]. Bone tissue engineering, which involves bone formation or regeneration using scaffolds for restoration and maintenance, is becoming increasingly popular for treating bone defects [2]. It is necessary to create an essential environment by mimicking the extracellular matrix (ECM) properties of natural bone and bone structures. Therefore, bone scaffolds require bioactive factors that can stimulate bone remodeling and structures that can support the formation of a new bone and then degrade as the new bone is produced [3].

Scaffolds for bone tissue engineering must have an interconnected structure. The structure should be able to transfer oxygen and nutrients, construct new vessels through pores, and mimic the bone structure of an individual patient [2–4]. Bioprinting is one of the methods used to control the porosity and microstructure of a scaffold, including its shape and pore size [1,3] In addition, materials that can be used as bone scaffolds need to be absorbed safely into the body during the progression of osteogenesis [5]. Polycaprolactone (PCL) is a good material for 3D printing, exhibiting excellent biodegradability, biocompatibility, and processability [6]. However, it lacks surface bioactivity and cell–scaffold interactions such as cell adhesion and osteoinduction. The PCL polymer is hydrophobic, which hinders the penetration of cell suspensions [5]. In addition, the acidic degradation of PCL affects the surrounding tissues and increases the likelihood of inflammation [7]. To overcome the bioactivity limitations, some studies have introduced biologically active functional groups or materials such as chitosan into synthetic polymers [7]. Furthermore, some studies have increased the surface area or wettability by controlling the roughness via composite scaffolds using hydroxyapatite and calcium carbonate [8,9].

Marine organisms have attracted considerable research interest for use in bone scaffolds because they are a source of osteogenic bioactive substances that promote new bone formation [10]. Marine organisms have a complex composition, and the process of biomineralization exhibits characteristics similar to those required for human bone formation [11–13]. Abalone, which is a group of marine gastropod mollusks, exhibits biocompatibility, slow biodegradability, and osteogenic ability [14]. Abalone shells contain approximately 95%–97% inorganic materials such as calcium carbonate and 3%–5% organic materials. Calcium carbonate is a crystallographic form of $CaCO_3$, with calcite in the outer layer and aragonite in the inner layer (nacre) [12,14,15]. The nacre calcified structures that form the lustrous inner layer have an organic matrix that is mainly composed of proteins and polysaccharides. Nacre consists of a brick-and-mortar microstructure, with aragonite serving as bricks and organic matter such as chitosan as the mortar [12,16]. Therefore, a thin sheet of aragonite is covered by an organic matrix [17]. Water soluble matrix (WSM), which constitutes the macromolecules of the nacre organic matrix, has been investigated for its effects on cells [18]. Nacreous factors contained in the WSM of nacre have beneficial effects on bone regeneration. Studies have shown that they positively affect the proliferation and differentiation of osteoblast cells [17,19], and the possibility of using marine shell for bone defect treatment has been reported. Scaffolds have been fabricated by electrospinning and bioprinting of blended polymers and shell powders [18,20]. Other studies have shown the possibility of developing bone-repair materials by mimicking the formation of ASPs [9].

In this study, abalone shells, which can assist in bone regeneration, were thermally embedded into a biodegradable PCL scaffold to form a bone scaffold. Abalone shells contain organic materials that could support osteogenesis as bioactive matter and inorganic materials that could enhance the mechanical properties and change the surface roughness to compensate for the limitations of the PCL scaffold. In addition, this study investigated the effectiveness of using abalone shell particles (ASPs) in bone scaffolds via a very simple process that only involves heat application to the ASPs. The cell viability, proliferation, and differentiation of the osteoblast-like MG63 cell-line on the ASPs was investigated (Fig. 1).

2. Materials and methods

2.1. Preparation of abalone particles

The abalone shells were thoroughly washed, and the shell, skin, and meat were separated. The abalone shells used in the experiment underwent high-temperature processing. ASPs were dried and transferred into an electrical furnace heated at a rate of 10 °C/min and calcined at 300 °C for 8 h. The processed ASPs were evenly filtered before use.

2.2. Preparation of ASP scaffolds

2.2.1. Fabrication and design of PCL scaffold

The PCL scaffold was fabricated using a 3D bioprinter (PROTEK, Korea Institute of Machinery and Materials, Korea). This bioprinter was based on the Fused Deposition Modeling (FDM) method. PCL pellets (MW: 45 k; Sigma-Aldrich, USA) were melted in a stainless steel cylindrical barrel, which was heated to a temperature greater than the melting point of PCL (100 °C) by using a heating jacket. Air pressure was maintained at approximately 350–420 kPa for printing. The strand size of the scaffold was set using a 400 μm diameter nozzle, and the gaps between strands were set at 400 μm. The scaffold size was 5 mm × 5 mm × 3 mm (W × D × H) for cell culture studies.

2.2.2. Thermally embedding ASPs in PCL scaffold

The following process was performed to thermally embed the ASPs in the fabricated PCL scaffold. First, 25 mg (ASP25), 50 mg (ASP50), and 100 mg (ASP100) quantities of the ASPs were placed in tubes and heated using a heating block (HB-R; WiseTherm, USA) at 80 °C. A temperature of 80 °C, which was a temperature close to the melting point of PCL, was used to fix the particles by slightly melting the PCL. The scaffold was not damaged at this temperature, and the number of ASPs could be controlled by maintaining their weight [S1]. The tube was placed in the heating block for at least 5 min to allow sufficient heat conduction to the particles. Next, the printed PCL scaffold was placed into the tube containing the heated ASPs and shaken up and down 50 times to evenly distribute and embed the particles in the scaffold. The number of the embedded ASPs in the scaffolds varied when the tube was shaken<20

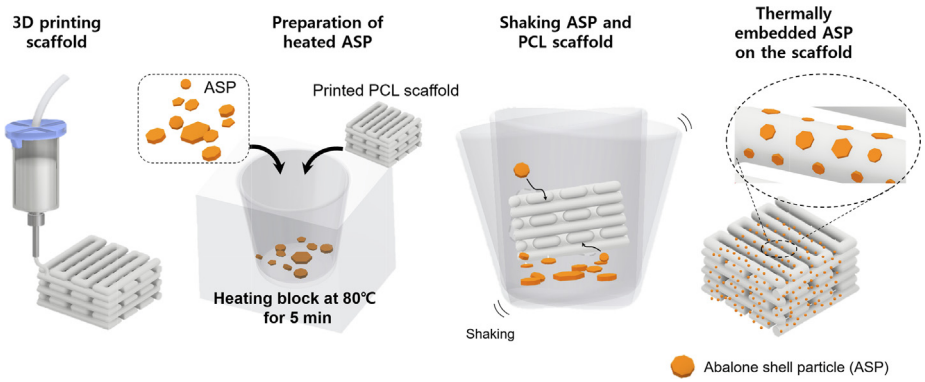

Fig. 1. Schematic illustration of the fabrication of the ASP scaffold. The PCL scaffold was printed using 3D bioprinting. ASPs were then placed into a tube in the heating block and heated at 80 °C until the heat conduction was complete. Thereafter, the PCL scaffold was placed into the same tube and shaken to thermally embed the ASPs in the scaffold.

times. Thus, the tubes were sufficiently shaken 50 times to ensure uniform dispersion throughout the scaffold [S1].

2.3. Characterization of ASP scaffolds

2.3.1. Scanning electron microscopy (SEM) and surface roughness analysis

SEM (Sirion; FEI, USA) was conducted to investigate the surface morphology of the scaffold. A sputter-coating device (SCD 005; BAL-TEC, Liechtenstein) was used for 3 min at 30 mA to coat the ASP scaffold with gold.

The surface roughness of the scaffold was measured using a surface measuring system (SV-3200; Mitutoyo, Japan). The sampling length was set to 2.8 mm, and the measurement proceeded as follows. The scaffold was placed on the positioning table with the upper part set in the upward direction. The crank shaft was placed in a downward orientation to measure the roughness of the top surface of the scaffold. The roughness was calculated as the arithmetic mean roughness (Ra), which represented the average absolute distance in the direction of the normal vector to the section curve of the surface based on the centerline average within the sampling length.

2.3.2. Water contact angle of ASP scaffold

A contact angle meter (Contact Angle Meter DM 210; Kyowa, Japan) was used to measure the hydrophilicity of the scaffold with embedded ASPs. Distilled water (DW) (5 μL) was placed on the scaffold surface, and the contact angle was measured after 1 min by capturing the side of the scaffold.

2.4. Chemical construction of ASP scaffold

2.4.1. Fourier-transform infrared spectroscopy and energy-dispersive X-ray spectroscopy

The chemical composition of the ASP scaffold was analyzed through Fourier-transform infrared (FTIR) spectroscopy (NICOLET 6700; Thermo Fisher Scientific, USA) with a resolution of 2 cm^{-1}. Energy-dispersive X-ray spectroscopy (EDX, OCTANE PRO; AMETEK, Japan) was performed for the elemental analysis of each scaffold sample. The EDX system was connected to the SEM system for electron beam excitation.

2.5. Mechanical properties

The compressive strength was measured with a universal testing machine (RB301 UNITECH-M; RnB, Korea) using a 500 kN load cell at a crosshead speed of 5 mm/min. A 5 × 5 × 3 mm scaffold was placed between the square jigs, and force was applied (Fig. 5 (a)). The compression test results were used to plot a stress–strain curve, and the Young's modulus and toughness values were measured.

2.6. Cell culture

MG63 cells were used for the cell assays of the scaffolds. The cells were cultured in Dulbecco's Modified Eagle's Medium (HyClone, USA) supplemented with 10% Fetal Bovine Serum (FBS) and 1% penicillin. All the scaffolds were sterilized by soaking in 70% ethanol for 1 min and washed with phosphate buffered saline (PBS) to remove the ethanol. A total of 5 × 10^5 cells per scaffold were seeded onto the sterilized scaffold on a clean bench. The scaffolds were cultured at 37 °C and 5% CO_2. The medium was changed every 2–3 d. Osteogenic differentiation induction medium, alpha MEM supplemented with 10% FBS, 1% penicillin, 50 μg mL^{-1} ascorbic acid, 10 mM of of β-glycerophosphate, and 10 nM dexamethasone, were used for differentiation assay.

2.7. Cell viability assay

The LIVE/DEAD viability assay kit (LIVE/DEAD™ Viability/Cytotoxicity Kit; Invitrogen, USA) was used to investigate the cell viability in the ASP scaffold. The cultured scaffolds were washed with PBS to remove the medium. The cells were stained with a dyeing solution containing calcein AM and ethidium homodimer-10 at 37 °C for 30 min. The live and dead cells of the ASP scaffold were observed using a fluorescence microscope (Eclipse Ti; Nikon, Japan).

Cell morphology on the ASP groups were investigated by SEM. The scaffolds were cultured for 7 days and the medium changed every 2 days. After incubation, the groups with and without ASP were washed with PBS. The cells attached on the surface of the scaffolds were fixed with 2.5% glutaraldehyde solution for 2 h at room temperature. The cells were dehydrated through ethanol graded series (30, 50, 70, 90 and 100 %) for about 15 min each and the scaffolds left to dry in a clean bench at room temperature. The scaffolds were coated with gold by a sputter-coating device and investigated by SEM.

2.8. Cell proliferation, alkaline phosphatase (ALP) activity and mineralization assays

Cell proliferation was investigated using the WST-1 cell proliferation assay (Premix WST-1 Cell Proliferation Assay System; Takara, Japan). The medium and WST-1 solutions were mixed in a 10:1 ratio to prepare a dyeing solution. The scaffolds were washed with PBS and moved to a new 48-well plate. Next, 500 μL of the dyeing solution per well was added and incubated

for 30 min. The extracted dyeing solution was added to a new 96-well plate, and the absorbance was measured at 450 nm using a microplate reader (SpectraMax iD3; Molecular Devices, USA). WST-1 investigations were performed after 4 and 7 d.

ALP activity was used to analyze the osteogenic differentiation [21]. The ASP scaffolds were washed with PBS. Thereafter, the cells of the scaffolds were lysed with the extraction solution (Pierce RIPA buffer; Thermo Fisher Scientific, USA) and maintained at − 80 °C until further use. Samples were exposed to freeze–thaw cycles and centrifuged, after which the supernatant was added to the p-NPP solution (TRACP & ALP Assay Kit; Takara, Japan). The enzyme was allowed to react at 37 °C for 30 min. After incubation, 50 μL of the stop solution (0.9 NaOH) was added to the samples, and the absorbance was measured at 405 nm using a microplate reader. The ALP activity was normalized by a PicoGreen dsDNA assay (Quant-iT™ PicoGreen™ dsDNA Assay Kit; Invitrogen, USA), and the results were directly related to the cell number [22,23].

Alizarin red staining (ARS) was used to investigate the ASP scaffolds assist mineralization of osteoblast cells. Cells were cultured in differentiation induction medium for 7 days. The samples were washed with DW three times. The differentiated cells were fixed with 4% paraformaldehyde at 25 °C. After 20 min, cells were washed with DW twice. The ASP scaffolds with cells were stained in ARS solution for 45 min in dark. After staining, the samples were investigated that cells were stained with ARS, which can stain calcium to verify mineralization.

2.9. Statistical analysis

All of the quantitative data are presented as the mean ± standard deviation. The results were analyzed using a one-way analysis of variance followed by Tukey's post hoc test. The statistical significance was set at $p < 0.05$, as indicated by one asterisk in the figures. Statistical analysis was conducted using Origin (Origin 8.6 ver., OriginLab Corporation, USA).

3. Results

3.1. Characterization of ASP scaffolds

3.1.1. Morphology and roughness

An SEM image revealed whether the abalone particles were evenly embedded. Fig. 2(a) and (b) were taken at magnifications of 200 × and 1000×, respectively. The amount of ASPs in a strand is shown in Fig. 2(a). As the weight of the ASPs increased, the number of ASPs fixed on the strand increased, and they were found to be evenly distributed. Fig. 2(b) depicts the morphology of the ASPs and how they were embedded in PCL. The ASPs used in the experiment contained the prismatic layer and nacre layer of the shell. In particular, the nacre layer contained a brick-and-mortar microstructure, as shown in Fig. 2(b). The shape of a plate with a broken layered structure was revealed [18]. A large number of particles were embedded on the surface as the weight of the ASPs increased. Additionally, it was found that the ASPs were evenly distributed on the inner layer of the scaffold, as seen in Fig. 2(c), and the number of ASPs could be controlled.

A change in the roughness of the scaffold influenced the biological response. The cell orientation, cell migration, and cytoskeletal function were directly affected by the surface roughness [24,25]. In particular, the cytokine and growth factor production of MG63, an osteoblast-like cell, were affected, suggesting that the proliferation, differentiation, and matrix production of cells were modulated by the surface roughness [26]. The arithmetic mean roughness (Ra) was used to measure the surface roughness. The PCL, ASP25, ASP50, and ASP100 scaffolds are shown in Fig. 3. The Ra value of the ASP100 scaffold was the highest at 7.07 μm. The Ra values of ASP50, ASP25, and PCL were 5.40, 4.82, and 3.52 μm, respectively. The results show that increasing the weight of the ASPs increased the number of particles embedded in the scaffold. Accordingly, it was confirmed that the roughness increased. It has been reported that a surface roughness of 4–5 μm can induce adhesion in MG63 cells [26]. Increasing the roughness can enhance hydrophilicity, which can impede the penetration of cell suspensions and enhance the absorption of cell proteins [27,28].

3.1.2. Hydrophilic characterization

A hydrophilic surface can enhance protein absorption, which assists in cell attachment and cell growth and increases biocompatibility [25,27]. In this study, the ASPs increased wettability while creating heterogeneous surfaces [24,28]. Fig. 3(b) depicts the water contact with different scaffolds 1 min after the droplet was dropped. The contact angles for the PCL and ASP groups were measured and found to be 77.93° and 0°, respectively. These results showed that the scaffolds with ASPs embedded on their surfaces became hydrophilic. As the roughness increased, the hydrophilicity

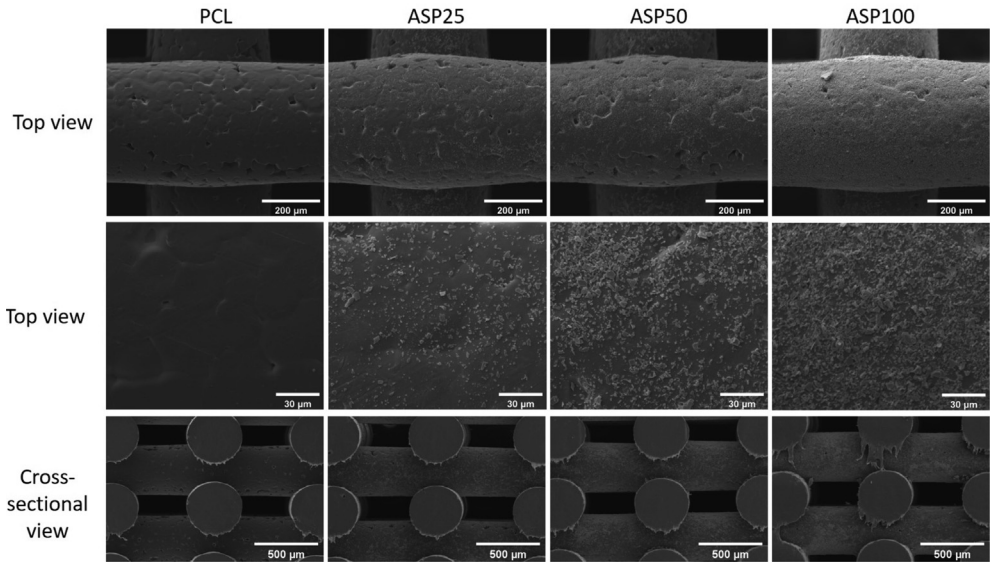

Fig. 2. SEM images showing top views of surface morphology and cross-sections of the ASP scaffolds.

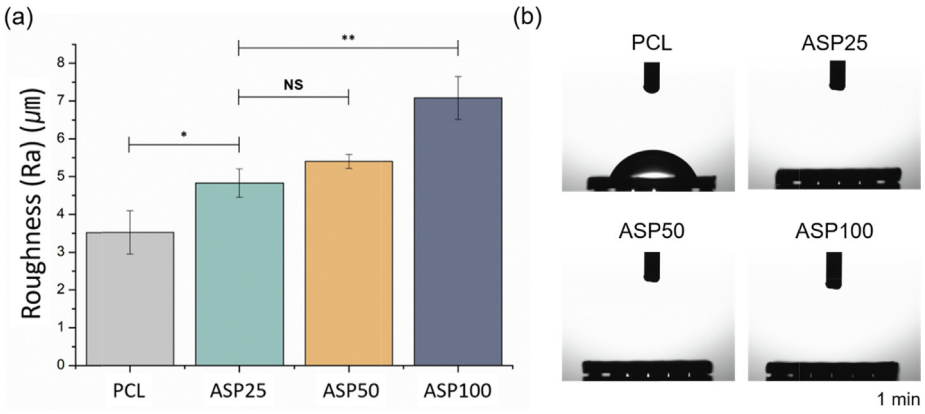

Fig. 3. Scaffold surface roughness and hydrophilicity: (a) arithmetic mean roughness (Ra) values of scaffolds [n = 3, NS: no significant difference, *p < 0.05 and **p < 0.01], and (b) wettability measurements of scaffolds.

increased, and it was assumed that the cell adhesion strengthened [24,25,27,28].

3.2. Chemical characterization of ASP scaffolds

3.2.1. FTIR and EDX analyses

The FTIR spectra of the thermally embedded ASP scaffolds are shown in Fig. 4. The characteristic peaks of PCL were observed at 2943 cm^{-1} (-C-H asymmetric stretching), 1722 cm^{-1} (-C = O stretching), and 1164 cm^{-1} (C-O-C) [29,30]. The FTIR spectrum of the ASP groups also showed the characteristic PCL peaks. The peaks for calcite at 1444, 1083, and 862 cm^{-1} commonly appeared in the ASP groups. The prismatic layer of the abalone shell contains the calcite form of calcium carbonate ($CaCO_3^{2-}$). The peak at 713 cm^{-1} was attributed to the aragonite form of calcium carbonate, which is present in the nacre layer [9,11,31]. Aragonite is transformed to calcite at temperatures greater than 300–400 °C through a process called mineral change [11].

In addition, the C-H peak at 2989 cm^{-1} only appeared in the spectra of the ASP groups; this peak is commonly associated with organic matter. Therefore, it can be assumed that the ASPs contained minimal organic matter [11,31]. It has been reported that the organic matrix in nacre is destroyed at ~ 500–600 °C, which is the temperature at which the mineral is transformed to calcium oxide, because of the strong interaction of the organic matrix with the mineral phase in the shell [11]. Therefore, the organic matrix remained after the processing method for the ASPs. This organic matrix contained bioactive molecules such as growth factors that could stimulate cell adhesion and proliferation [12,13,17].

In Table 1, the EDX results of PCL without ASPs and the three groups of ASPs are listed. The C and O signals were observed in both PCL and the ASP groups. Because $CaCO_3$ was a major component of the ASPs, the $CaCO_3$ peak for ASP100 exhibited the highest Ca intensity because it had the largest number of ASPs. In addition, the Pt signal appeared as a peak because a Pt coating was applied for EDX.

3.3. Mechanical properties

Fig. 5 shows the mechanical properties of the ASP scaffolds. The stress–strain curves are plotted in Fig. 5(b). These curves indicate that the mechanical properties of the scaffolds differed depending on the presence and number of ASPs. The curves were divided into an elastic deformation section that was relatively linear and a plastic deformation section. In the elastic deformation section, the Young's moduli of the PCL, ASP25, ASP50, and ASP100 scaffolds were 40.99, 37.36, 33.99, and 31.48 MPa, respectively (Fig. 5(c)). The PCL scaffold without particles had the highest stiffness, but the stiffness tended to decrease as the number of ASPs increased. The structure of the object influences the stiffness [32,33]. As the number of ASPs increased, the stiffness and strength at the yield point decreased. This loss of strength occurred because a shape

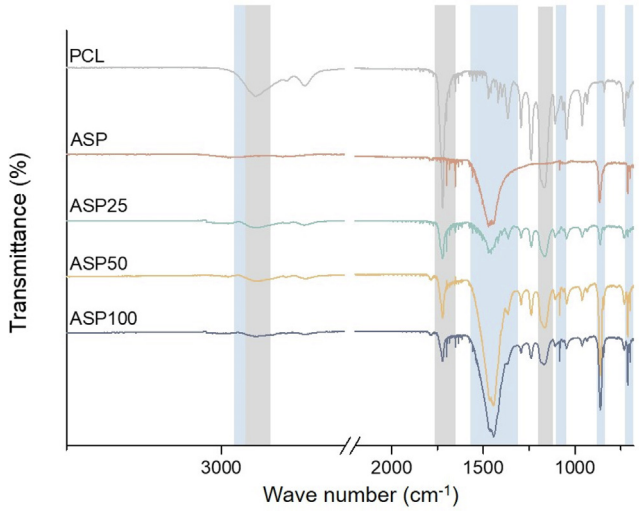

Fig. 4. FTIR results for PCL scaffold, ASPs, and ASP scaffolds.

Table 1
EDX results for the PCL and ASP scaffolds.

Sample	Element	Weight (%)	Atomic (%)
PCL	C K	43.63	54.67
	O K	46.62	43.85
	Pt M	7.30	0.56
	Ca K	2.45	0.92
ASP25	C K	13.68	21.12
	O K	58.31	67.58
	Pt M	4.51	0.43
	Ca K	23.51	10.88
ASP50	C K	4.53	7.77
	O K	58.06	74.77
	Pt M	4.33	0.46
	Ca K	33.07	17.00
ASP100	C K	6.78	11.85
	O K	51.96	68.12
	Pt M	3.75	0.40
	Ca K	37.51	19.63

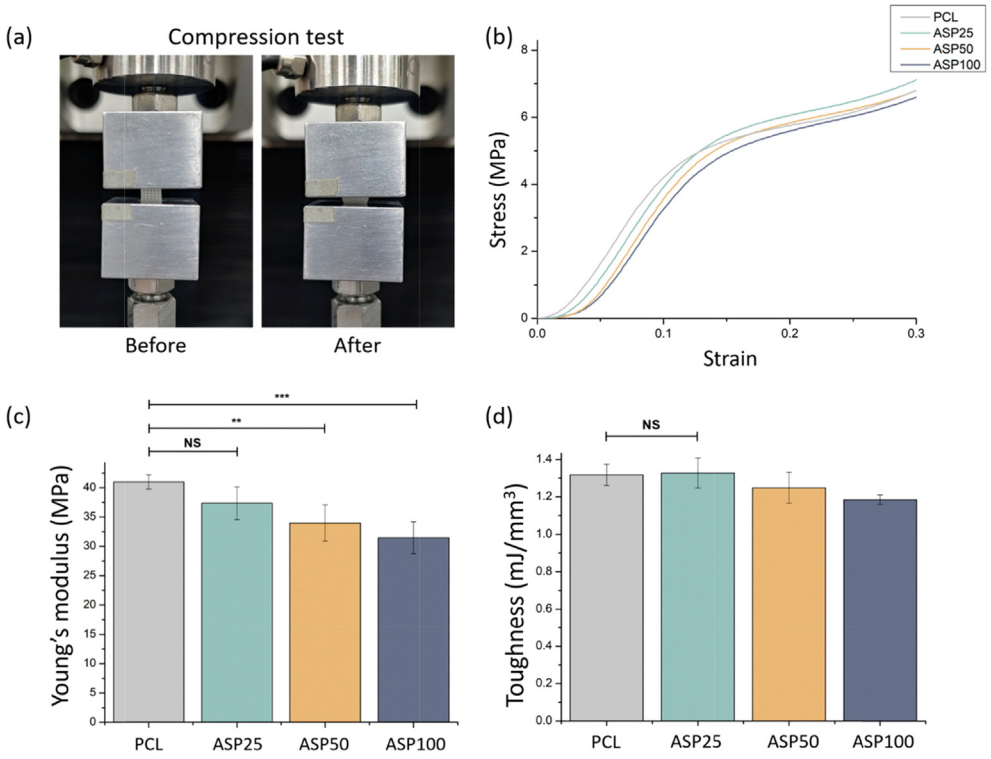

Fig. 5. Mechanical properties of PCL, ASP25, ASP50, and ASP100: (a) photograph of compression test, (b) stress–strain curves, (c) Young's modulus values [n = 3, NS: no significant difference, $^{**}p < 0.01$ and $^{***}p < 0.001$], and (d) toughness values of scaffolds.

change occurred, with many holes formed in the polymer structure. When stress greater than the yield point was applied, different characteristics were observed as the stress entered the plastic deformation section. The strains for the ASP25 and ASP50 groups were smaller than that of the PCL scaffold. As the scaffolds were compressed, a continuous change occurred in the plastic deformation section. As the particles became closer to each other, the arrangement became denser. As the number of contact points between the ASPs increased, the compressive pressure dispersed. This enabled a higher resistance to compression [34].

However, in the ASP100 group, the resistance to compression was lower than that in the PCL scaffold. The presence of too many particles in the ASP100 scaffold caused them to crush each other, which affected force distribution [35].

Fig. 5(d) shows the toughness values of the scaffolds when the strain was 0.3%. Toughness is defined as the amount of energy that a material can absorb until just before cracking occurs without fracture. The toughness values of the PCL, ASP25, ASP50, and ASP100 scaffolds were 1.318, 1.328, 1.248, and 1.185 mJ/mm^3, respectively. ASP25 exhibited the highest toughness, whereas ASP100 had the lowest. Thus, an appropriate number of ASPs could slightly increase toughness.

3.4. Cell viability

Live and dead assays were performed to investigate the attachment and viability of the MG63 cells seeded on the scaffold. Fig. 6 (a) shows cells stained for the live and dead assay 1 and 7 d after the seeding of cells. On days 1 and 7, the ASP groups had higher cell viability than the PCL. On day 7, the ASP25 group had the highest cell viability. Fig. 6 (b) shows cells were observed to be more attached to the ASP scaffolds compared with the cells of the PCL scaffold. Especially, the ASP25 and ASP 50 groups are covered with cells.

This was most likely influenced by changes in the rough surface and pH. The roughness directly affected the cytoskeleton of the cell and cell attachment [24,25]. In particular, a surface with Ra values in the range of 4–5 μm favored MG63 cells [36]. In addition, roughness is one of the factors that can modify the wettability, which helps to transfer oxygen and nutrients and absorb proteins related to biocompatibility [24,25,27,28]. The ASP25 and ASP50 groups on day 1 had roughness values in the range of 4–5 μm, and more cell attachment was observed in the ASP groups. In addition, when each group of scaffolds was placed in PBS and observed for 3 d, it was confirmed that the pH value was higher in a group with more ASPs [S2]. The change in pH was due to the dissolution of $CaCO_3$, and a rapid change in pH inhibited cell proliferation [18]. A sudden change in pH occurred in the groups with high ASP ratios (ASP100 and ASP50), and a relatively large number of dead cells were identified. This could be explained by the fact that the ASP25 group had the highest viability because of the optimal pH value.

3.5. Cell proliferation, differentiation and mineralization

The process of bone formation by osteoblasts involves mineralization through proliferation and differentiation [19,37]. Fig. 7(a) shows the WST-1 results, which were used to evaluate the cell proliferation on days 4 and 7. In the WST-1 assay, the absorbance value increased with time, and the values for the ASP groups were higher than that of the PCL.

Fig. 7(b) shows the ALP assay results that were used to analyze the degree of differentiation by activating the early marker of bone differentiation after 4 and 7 d of incubation. The ALP activity tended to increase with time, and the highest value was observed in the ASP100 group, which had the largest amount of ASPs.

Bone mineralization is the process that minerals are deposited on the bone matrix for bone remodeling. It is known that osteoblasts aids to the deposition of calcium and phosphorus on the

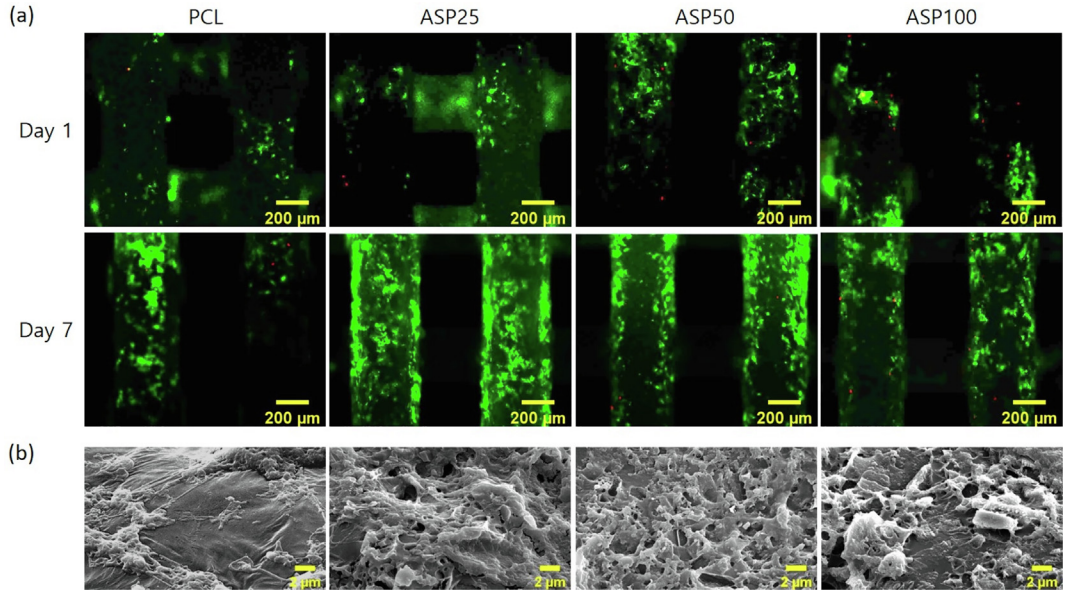

Fig. 6. Cell viability and morphology (a) Live and dead staining for investigating viability of MG63 cells. Cells were cultured on the scaffold for 1 and 7 d. (b) SEM image for investigating the cell morphology.

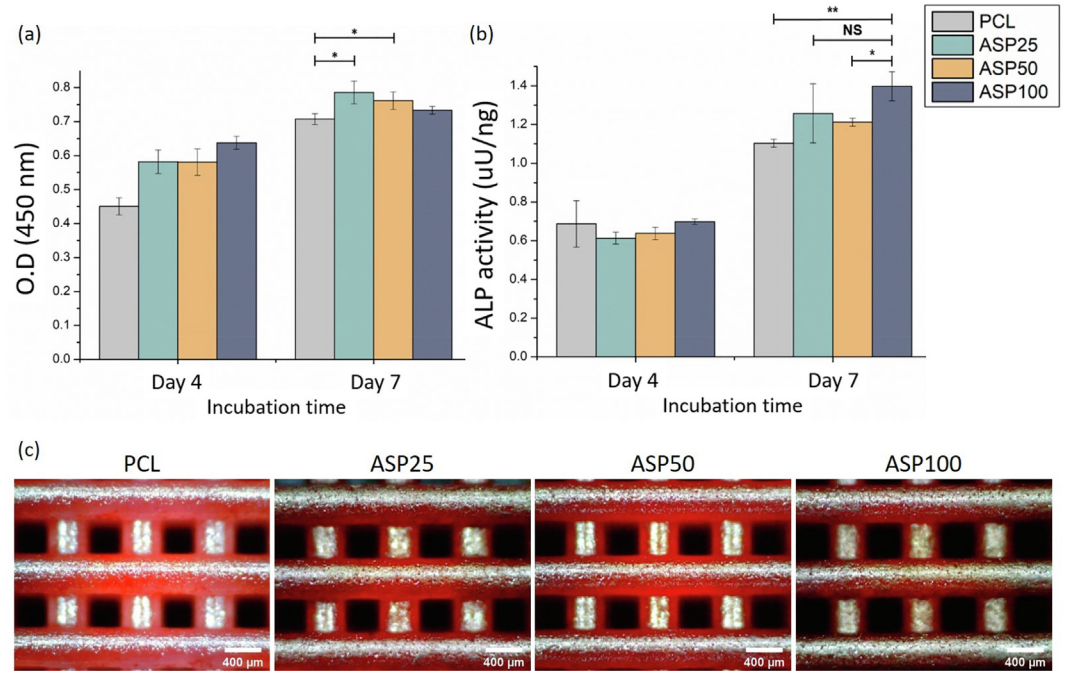

Fig. 7. Proliferation and differentiation of MG63 cells cultured on scaffolds for 4 and 7 d: (a) WST-1 assay results for MG63 cells on scaffold [n = 3, NS: no significant difference, *p < 0.05 and **p < 0.01] and (b) ALP activities of MG63 cells on scaffolds. (c) ARS staining of MG63 cells on scaffolds.

collagen-based fibrous matrix to form a hard inorganic substance called hydroxyapatite during the mineralization process. Therefore, bone mineralization can be investigated through calcium deposition after osteoblast differentiation. The scaffolds were measured using the ARS staining which is commonly used to detect calcium deposition. In the Fig. 7(c), it can be observed that the calcium deposition was highest in the ASP100 and ASP25. This tendency was similar to ALP, an early marker of osteodifferentiation.

This could be explained by the following factors. The first was the pH change due to calcium carbonate, which is the main inorganic component of abalone shells. Alkaline environments increase the activity of osteoblasts, promote bone formation and the mineralization of osteoblasts, and enhance differentiation through increased ALP activity and collagen synthesis [38,39]. In addition, calcium ions were released through the dissolution of calcium carbonate. Higher calcium ion concentrations promote the formation of cadherin to enhance osteodifferentiation, leading to favorable biocompatibility [40,41]. Another reason was the influence of WSM, which is the organic macromolecule matrix of the abalone shell. Many studies have shown that WSM affects the adhesion and proliferation of osteoblasts. Mineral-based organic structures consisting of bioactive molecules such as growth factors can sup-

port bone grafting and bone regeneration [17,18]. For these reasons, the highest ALP activity was observed in the ASP100 group, which had the largest number of abalone particles. This suggested that the ASPs could positively affect cell proliferation, differentiation and mineralization. However, there was not much difference in the differentiation values of the ASP100 and ASP25 groups. This was because the viability and proliferation tended to be superior in the ASP25 compared to the ASP100. Thus, it can be expected that the differentiation after proliferation would not show much difference.

4. Conclusions

Abalone shells have macromolecules that can promote osteogenesis and have been shown to be suitable for use in scaffolds as bioactive factors. In this study, ASP scaffolds were fabricated through a very simple process of heating the ASPs at an optimized temperature, and the resulting scaffolds were found to be advantageous. Through this process, a heterogeneous surface was created in all the groups. This increased the wettability, which affected the penetration of cell suspensions and enhanced the absorption of cell proteins. In particular, the ASP25 and ASP50 groups had a surface roughness of 4–5 μm, which could enhance the adhesion of MG63 cells. In addition, when the ASPs were embedded, the mechanical properties were changed by a change in the shape of PCL. However, compared to PCL, the toughness, which was the energy dissipated when pressure was applied, tended to increase slightly for ASP25. The best cell viability was observed in the ASP25 group, and this was due to the effect of changes in the pH and surface roughness. The ASP25 group had high cell proliferation on day 7. The ASP100 group, which contained the most ASPs, showed the best initial differentiation, as indicated by the ALP results. This tendency could be explained by the multiple influences of the pH, organic matter, and release of calcium ions. Based on the results for the mechanical properties, cell adhesion, proliferation, differentiation and mineralization, the ASP25 scaffold was found to be the most suitable for use in bone scaffolds. This study demonstrated the possibility of applying natural bio-organisms produced through a process similar to human bone formation to bone tissue engineering.

CRediT authorship contribution statement

Dahong Kim: Writing – original draft, Conceptualization. **Jihye Lee:** Conceptualization. **Ji Min Seok:** Methodology, Formal analysis. **Joo-Yun Jung:** Methodology, Formal analysis. **Jun Hee Lee:** Methodology, Formal analysis. **Jun Sik Lee:** Methodology, Formal analysis. **Kangwon Lee:** Supervision. **Su A Park:** Writing – review & editing, Supervision.

Declaration of Competing Interest

The authors declare that they have no known competing financial interests or personal relationships that could have appeared to influence the work reported in this paper.

Acknowledgements

This research was supported by the National Research Foundation (NRF), funded by the Korean government (MSIT; No. NRF-2019M3A9E2066348, 2020M3H4A1A02084828 and 2019M3E6A 1103999).

Appendix A. Supplementary material

Supplementary data to this article can be found online at https://doi.org/10.1016/j.matdes.2021.110228.

References

[1] S.R. Motamedian, Smart scaffolds in bone tissue engineering: A systematic review of literature, World J. Stem Cells 7 (3) (2015) 657, https://doi.org/10.4252/wjsc.v7.i3.657.
[2] M.M. Stevens, Biomaterials for bone tissue engineering, Mater. Today 11 (5) (2008) 18–25, https://doi.org/10.1016/S1369-7021(08)70086-5.
[3] S. Preethi Soundarya, A. Haritha Menon, S. Viji Chandran, N. Selvamurugan, Bone tissue engineering: Scaffold preparation using chitosan and other biomaterials with different design and fabrication techniques, Int. J. Biol. Macromol. 119 (2018) 1228–1239, https://doi.org/10.1016/j.ijbiomac.2018.08.056.
[4] G. Chiara, F. Letizia, F. Lorenzo, S. Edoardo, S. Diego, S. Stefano, B. Eriberto, Z. Barbara, Nanostructured biomaterials for tissue engineered bone tissue reconstruction, Int. J. Mol. Sci. 13 (1) (2012) 737–757, https://doi.org/10.3390/ijms13010737.
[5] M.A. Elnaggar, H.A.N. El-Fawal, N.K. Allam, Biocompatible PCL-nanofibers scaffold with immobilized fibronectin and laminin for neuronal tissue regeneration, Mater. Sci. Eng. C 119 (2021) 111550, https://doi.org/10.1016/j.msec.2020.111550.
[6] C. Murphy, K. Kolan, W. Li, J. Semon, D. Day, M. Leu, 3D bioprinting of stem cells and polymer/bioactive glass composite scaffolds for bone tissue engineering, Int. J. Bioprinting 3 (1) (2017) 53–63, https://doi.org/10.18063/IJB.2017.01.005.
[7] L. Yang, J. Li, Y. Jin, M. Li, Z. Gu, In vitro enzymatic degradation of the cross-linked poly(ε-caprolactone) implants, Polym. Degrad. Stab. 112 (2015) 10–19, https://doi.org/10.1016/j.polymdegradstab.2014.12.008.
[8] M.S. Saveleva, A.N. Ivanov, M.O. Kurtukova, V.S. Atkin, A.G. Ivanova, G.P. Lyubun, A.V. Martyukova, E.I. Cherevko, A.K. Sargsyan, A.S. Fedonnikov, I.A. Norkin, A.G. Skirtach, D.A. Gorin, B.V. Parakhonskiy, Hybrid PCL/CaCO3 scaffolds with capabilities of carrying biologically active molecules: Synthesis, loading and in vivo applications, Mater. Sci. Eng. C 85 (2018) 57–67, https://doi.org/10.1016/j.msec.2017.12.019.
[9] J. Chen, Z. Wen, S. Zhong, Z. Wang, J. Wu, Q. Zhang, Synthesis of hydroxyapatite nanorods from abalone shells via hydrothermal solid-state conversion, Mater. Des. 87 (2015) 445–449, https://doi.org/10.1016/j.matdes.2015.08.056.
[10] M. Carson, S. Clarke, Bioactive compounds from marine organisms: Potential for bone growth and healing, Mar. Drugs 16 (9) (2018) 340, https://doi.org/10.3390/md16090340.
[11] J. Balmain, B. Hannoyer, E. Lopez, Fourier transform infrared spectroscopy (FTIR) and X-ray diffraction analyses of mineral and organic matrix during heating of mother of pearl (Nacre) from the shell of the mollusc Pinctada maxima, J. Biomed. Mater. Res. 48 (5) (1999) 749–754, https://doi.org/10.1002/(SICI)1097-4636(1999)48:5<749::AID-JBM22>3.0.CO;2-P.
[12] E.M. Gerhard, W. Wang, C. Li, J. Guo, I.T. Ozbolat, K.M. Rahn, A.D. Armstrong, J. Xia, G. Qian, J. Yang, Design strategies and applications of nacre-based biomaterials, Acta Biomater. 54 (2017) 21–34, https://doi.org/10.1016/j.actbio.2017.03.003.
[13] T.Y. Chen, H.C. Huang, J.L. Cao, Y.J. Xin, W.F. Luo, N.J. Ao, Preparation and characterization of alginate/HACC/oyster shell powder biocomposite scaffolds for potential bone tissue engineering applications, RSC Adv. 6 (42) (2016) 35577–35588, https://doi.org/10.1039/c5ra26805b.
[14] V. Srot, U.G.K. Wegst, U. Salzberger, C.T. Koch, K. Hahn, P. Kopold, P.A. van Aken, Microstructure, chemistry, and electronic structure of natural hybrid composites in abalone shell, Micron 48 (2013) 54–64, https://doi.org/10.1016/j.micron.2013.02.010.
[15] A. Lin, M.A. Meyers, Growth and structure in abalone shell, Mater. Sci. Eng. A 390 (1–2) (2005) 27–41, https://doi.org/10.1016/j.msea.2004.06.072.
[16] J. Sun, B. Bhushan, Hierarchical structure and mechanical properties of nacre: A review, RSC Adv. 2 (20) (2012) 7617–7632, https://doi.org/10.1039/c2ra20218b.
[17] V. Agarwal, E.S. Tjandra, K.S. Iyer, B. Humfrey, M. Fear, F.M. Wood, S. Dunlop, C. L. Raston, Evaluating the effects of nacre on human skin and scar cells in culture, Toxicol. Res. (Camb) 3 (4) (2014) 223–227, https://doi.org/10.1039/C4TX00004H.
[18] Y. Liu, Q. Huang, Q. Feng, 3D scaffold of PLLA/pearl and PLLA/nacre powder for bone regeneration, Biomed. Mater. 8 (6) (2013) 065001, https://doi.org/10.1088/1748-6041/8/6/065001.
[19] H. Kim, K. Lee, C.-Y. Ko, H.-S. Kim, H.-I. Shin, T. Kim, S.H. Lee, D. Jeong, The role of nacreous factors in preventing osteoporotic bone loss through both osteoblast activation and osteoclast inactivation, Biomaterials 33 (30) (2012) 7489–7496, https://doi.org/10.1016/j.biomaterials.2012.06.098.
[20] R. Didekhani, M.R. Sohrabi, M. Soleimani, E. Seyedjafari, H. Hanaee-Ahvaz, Incorporating PCL nanofibers with oyster shell to improve osteogenic differentiation of mesenchymal stem cells, Polym. Bull. 77 (2) (2020) 701–715, https://doi.org/10.1007/s00289-019-02750-x.
[21] B. Reible, G. Schmidmaier, M. Prokscha, A. Moghaddam, F. Westhauser, Continuous stimulation with differentiation factors is necessary to enhance osteogenic differentiation of human mesenchymal stem cells in-vitro, Growth

Factors 35 (4–5) (Sep. 2017) 179–188, https://doi.org/10.1080/08977194.2017.1401618.
[22] X. Zhang, X. Du, D. Li, R. Ao, B. Yu, B. Yu, Three dimensionally printed pearl powder/poly-caprolactone composite scaffolds for bone regeneration**, J. Biomater. Sci. Polym. Ed. 29 (14) (2018) 1686–1700, https://doi.org/10.1080/09205063.2018.1475096.
[23] F. Westhauser, M. Karadjian, C. Essers, A.-S. Senger, S. Hagmann, G. Schmidmaier, A. Moghaddam, T. Webster, Osteogenic differentiation of mesenchymal stem cells is enhanced in a 45S5-supplemented β-TCP composite scaffold: An in-vitro comparison of Vitoss and Vitoss BA, PLoS ONE 14 (2) (2019) e0212799, https://doi.org/10.1371/journal.pone.0212799.
[24] J.I. Rosales-Leal, M.A. Rodríguez-Valverde, G. Mazzaglia, P.J. Ramón-Torregrosa, L. Díaz-Rodríguez, O. García-Martínez, M. Vallecillo-Capilla, C. Ruiz, M.A. Cabrerizo-Vílchez, Effect of roughness, wettability and morphology of engineered titanium surfaces on osteoblast-like cell adhesion, Colloids Surfaces A Physicochem. Eng. Asp. 365 (1-3) (2010) 222–229, https://doi.org/10.1016/j.colsurfa.2009.12.017.
[25] F. Rupp, L. Scheideler, D. Rehbein, D. Axmann, J. Geis-Gerstorfer, Roughness induced dynamic changes of wettability of acid etched titanium implant modifications, Biomaterials 25 (7–8) (2004) 1429–1438, https://doi.org/10.1016/j.biomaterials.2003.08.015.
[26] K. Kieswetter et al., Surface roughness modulates the local production of growth factors and cytokines by osteoblast-like MG-63 cells, J. Biomed. Mater. Res. 32 (1) (1996) 55–63, https://doi.org/10.1002/(SICI)1097-4636(199609)32:1<55::AID-JBM7>3.0.CO;2-O.
[27] E.S. Thian, Z. Ahmad, J. Huang, M.J. Edirisinghe, S.N. Jayasinghe, D.C. Ireland, R. A. Brooks, N. Rushton, W. Bonfield, S.M. Best, The role of surface wettability and surface charge of electrosprayed nanoapatites on the behaviour of osteoblasts, Acta Biomater. 6 (3) (2010) 750–755, https://doi.org/10.1016/j.actbio.2009.08.012.
[28] M.G. Orkoula, P.G. Koutsoukos, M. Robin, O. Vizika, L. Cuiec, Wettability of CaCO3 surfaces, Colloids Surfaces A Physicochem. Eng. Asp. 157 (1–3) (1999) 333–340, https://doi.org/10.1016/S0927-7757(99)00047-3.
[29] L. Ghasemi-Mobarakeh, M.P. Prabhakaran, M. Morshed, M.H. Nasr-Esfahani, S. Ramakrishna, Bio-functionalized PCL nanofibrous scaffolds for nerve tissue engineering, Mater. Sci. Eng. C 30 (8) (2010) 1129–1136, https://doi.org/10.1016/j.msec.2010.06.004.
[30] H. Yu, Y. Jia, C. Yao, Y. Lu, PCL/PEG core/sheath fibers with controlled drug release rate fabricated on the basis of a novel combined technique, Int. J. Pharm. 469 (1) (2014) 17–22, https://doi.org/10.1016/j.ijpharm.2014.04.045.
[31] S. Zhong, Z. Wen, J. Chen, Q. Li, X. Shi, S. Ding, Q. Zhang, Effects for rapid conversion from abalone shell to hydroxyapaptite nanosheets by ionic surfactants, Mater. Sci. Eng. C 77 (2017) 708–712, https://doi.org/10.1016/j.msec.2017.04.009.
[32] K. Hbaieb, Q.X. Wang, Y.H.J. Chia, B. Cotterell, Modelling stiffness of polymer/clay nanocomposites, Polymer (Guildf) 48 (3) (2007) 901–909, https://doi.org/10.1016/j.polymer.2006.11.062.
[33] N. Sheng, M.C. Boyce, D.M. Parks, G.C. Rutledge, J.I. Abes, R.E. Cohen, Multiscale micromechanical modeling of polymer/clay nanocomposites and the effective clay particle, Polymer (Guildf) 45 (2) (2004) 487–506, https://doi.org/10.1016/j.polymer.2003.10.100.
[34] M. Iskander, M. Omidvar, S. Bless, in: Rapid Penetration into Granular Media, Elsevier, 2015, pp. 11–63, https://doi.org/10.1016/B978-0-12-800868-3.00002-X.
[35] P.A.B. Poul, V. Lade, J.A. Yamamuro, Significance of particle crushing in granular materials, J. Geotech. Eng. 122(4) (1996) [Online]. Available: https://ascelibrary.org/doi/10.1061/%28ASCE%290733-9410%281996%29122%3A4%28309%29.
[36] M. Bachle, R.J. Kohal, A systematic review of the influence of different titanium surfaces on proliferation, differentiation and protein synthesis of osteoblast-like MG63 cells, Clin. Oral Implants Res. 15 (6) (2004) 683–692, https://doi.org/10.1111/j.1600-0501.2004.01054.x.
[37] C. Loty, J.M. Sautier, H. Boulekbache, T. Kokubo, H.M. Kim, N. Forest, In vitro bone formation on a bone-like apatite layer prepared by a biomimetic process on a bioactive glass-ceramic, J. Biomed. Mater. Res. 49 (4) (2000) 423–434, https://doi.org/10.1002/(SICI)1097-4636(20000315)49:4<423::AID-JBM1>3.0.CO;2-7.
[38] D.H. Kohn, M. Sarmadi, J.I. Helman, P.H. Krebsbach, Effects of pH on human bone marrow stromal cells in vitro: Implications for tissue engineering of bone, J. Biomed. Mater. Res. 60 (2) (2002) 292–299, https://doi.org/10.1002/jbm.10050.
[39] T.R. Arnett, Extracellular pH regulates bone cell function, J. Nutr. 138 (2) (2008) 415–418, https://doi.org/10.1093/jn/138.2.415s.
[40] Y.i. Liu, T. Jiang, Y.i. Zhou, Z. Zhang, Z. Wang, H. Tong, X. Shen, Y. Wang, Evaluation of the attachment, proliferation, and differentiation of osteoblast on a calcium carbonate coating on titanium surface, Mater. Sci. Eng. C 31 (5) (2011) 1055–1061, https://doi.org/10.1016/j.msec.2011.03.003.
[41] S. Maeno, Y. Niki, H. Matsumoto, H. Morioka, T. Yatabe, A. Funayama, Y. Toyama, T. Taguchi, J. Tanaka, The effect of calcium ion concentration on osteoblast viability, proliferation and differentiation in monolayer and 3D culture, Biomaterials 26 (23) (2005) 4847–4855, https://doi.org/10.1016/j.biomaterials.2005.01.006.